PHYSICAL REVIEW B VOLUME 29, NUMBER 5 1 MARCH 1984

Equation of state and metallization of CsI

John Aidun* and M. S. T. Bukowinski
Department of Geology and Geophysics, University of California, Berkeley, California 94720

Marvin Ross
Lawrence Livermore Laboratory, University of California, Livermore, California 94550

(Received 19 September 1983)

Self-consistent, nonrelativistic augmented-plane-wave (APW) calculations for CsI were carried out to generate the band structure, the static-lattice equation of state (EOS), and the volume dependence of the electronic energy-band gap. The theoretical room-temperature isothermal compression curve agrees well with static and ultrasonic measurements at low pressure. Our calculations do not agree with two recent sets of diamond-anvil-cell measurements above 10 GPa. The calculated band gaps are too small at low pressure, but, at high pressure, are consistent with both the experimental results and the Herzfeld-model prediction. These results suggest that the insulator-to-metal transition occurs in the range 100±10 GPa. A calculation of the shock compression curve of CsI shows that the thermally excited electrons cause a significant softening of the Hugoniot curve. The experimental zero-pressure band gaps of the isoelectronic compounds Xe, CsI, and BaTe are linearly correlated with $\ln(v/v_H)$, where v_H is the specific volume of metallization predicted by the Herzfeld model. Based on this correlation, and on the similarity of the APW calculated EOS's of Xe and CsI, which agree closely with experimental compression measurements, we predict that BaTe will become metallic at approximately 30 GPa.

I. INTRODUCTION

There is currently great interest in the pressure-induced insulator-to-metal transitions (IMT's) in the isoelectronic sequence Xe, CsI, and BaTe. In these compounds, electronic band-structure calculations suggest that the IMT's will proceed by a reordering of the energy bands,[1] with the empty *d*-like band dropping in energy below the top of the filled *p*-like bands. Augmented-plane-wave (APW) calculations predict that Xe will become metallic above 130 GPa (1.3 Mbar), at a volume very near the Herzfeld-theory prediction of 10.2 cm^3/mole (16.94 Å^3).[2–4] The predicted narrowing of the band gap has been found in very good agreement with diamond-anvil cell (DAC) optical measurements to 55 GPa.[5,6] These results are consistent with shock data for Xe in which it is found that the high temperatures accompanying the shock process ($\sim$30 000 K near 130 GPa) thermally excite electrons from the $5p$ to $5d$ states, and lead to a softening of the Hugoniot curve that depends on both the electron energy-band gap and its volume derivative.

In CsI metallization is expected to occur when the lowest unoccupied level, the $5d$-like cesium band, drops in energy below the top of the filled $5p$-like iodine band. In a previous paper[7] we compared a purely theoretical estimate of the metallization pressure in CsI with an estimate based on recent optical-absorption measurements,[8] and with the prediction of Herzfeld's theory.[4] We found our results to be consistent with both of these earlier values. In the present paper we give a more extensive discussion of the equation of state (EOS), and the volume dependence of the band gap, and present new calculations of the CsI Hugoniot curve.

We begin by giving, in Sec. II, details of the calculations of the electronic band structure, room-temperature compression curve, and zero-pressure mechanical properties. In Sec. III these results are compared with available experimental data, and we compare our calculated Hugoniot curves with the shock-compression data. Some final remarks are contained in Sec. IV.

II. METHOD OF CALCULATION

A. Contributions to the room-temperature pressure

The electronic band structure and the static-lattice EOS were calculated using the nonrelativistic, self-consistent, APW method.[9] These calculations used only the "muffin-tin" (MT) portion of the total crystal potential and the Hedin-Lundqvist (HL) model[10] for the exchange-correlation interaction. Since this model is known to give zero-pressure optical gaps that are too small,[2] calculations were also made using Slater's ($\alpha=1$) exchange potential.[11]

While relativistic effects are important in CsI, the good agreement with static-compression measurements at low pressures suggest that the relativistic corrections to the compressibility are small. Similarly, the correction for the effect of relativistic interactions on the band gap at zero pressure is small compared to the error inherent in the use of the electron-density-functional formalsim for the calculation of conduction bands.[12] On the basis of free-atom calculations[13] Ross and McMahan[2] estimated relativistic corrections to the band gap for Xe to be less than 0.5 eV. At high pressure, when the gap is very narrow, the effect of relativistic interactions may be appreciable, introducing a measure of uncertainty into our prediction of metallization. Electronic wave functions in the first four shells do not overlap significantly with neighbors and are, therefore, regarded as core states and treated as in a self-consistent atomic calculation. The remaining 16 electrons from the fifth shells of Cs^+ and I^- are treated as valence electrons for which Bloch function solutions are determined. These eigenvalues and eigenfunctions are calculated self-consistently on a mesh equivalent to 64 points in the full Brillouin zone. In the HL calculation, iteration of the solution was stopped when the successive changes in the pressure became less than 0.05 GPa at low pressures and less than 0.1 GPa at high pressures. The band energies in this calculation were correspondingly converged to better than 0.1 mRy. We used twelve angular momentum components in the spherical harmonic expansion for the wave function within the MT spheres, and omitted vectors longer than $6\pi/a$ from the reciprocal-lattice vector expansion, where a is the lattice constant. In the Slater calculation, band energies were iteratively converged to better than 1 mRy. No corrections to the band energies were made for the effects of the non-muffin-tin (NMT) portion of the crystal potential, nor for the effects of nonzero temperatures.

The room-temperature pressure at a given specific volume v may be expressed as

$$P(v,T_r)=P_{\text{APW}}+P_{\text{MT}}+P_0+P_{\text{th}} \tag{1}$$

with

$$P_{\text{APW}}(v)=P_{kC}+P_{\text{xc}} \ . \tag{2}$$

P_{APW} comprises the pressure arising from the electronic kinetic energy T, the Coulomb potential energy E_C, and the exchange-correlation energy E_{xc}, of the crystal, in the MT approximation. The first two contributions are given by the virial theorem,[14]

$$P_{kC}=(2T+E_C)/3v \ . \tag{3}$$

The exchange-correlation pressure P_{xc} is given as the volume derivative of the exchange-correlation energy

$$P_{\text{xc}}=-\frac{\partial}{\partial v}\int \rho E_{\text{xc}}dv \ . \tag{4}$$

By introducing scaled coordinates x such that $r=V^{1/3}x$, Eq. (4) is easily reduced to

$$P_{\text{xc}}=\frac{1}{v}\int \rho(V_{\text{xc}}-E_{\text{xc}})dv \ , \tag{5}$$

where ρ is the electronic charge density, V_{xc} is the exchange-correlation potential, and E_{xc} is the exchange-correlation energy per electron.[10] These latter two are related by a functional derivative,

$$V_{\text{xc}}(v)=\frac{d}{d\rho}(\rho E_{\text{xc}}) \ . \tag{6}$$

For the HL potential

$$V_{\text{xc}}(v)=-(e^2/\pi)(3\pi^2\rho)^{1/3}[1+Bx\ln(1+1/x)] \tag{7}$$

and for the Slater $(\alpha=1)$ potential

$$V_{\text{xc}}(v)=-(3e^2/2\pi)(3\pi^2\rho)^{1/3} \ . \tag{8}$$

In Eq. (7) x is the radius of a sphere whose volume is $1/\rho$, the volume per electron, divided by a constant A. Following Lundqvist and Lundqvist,[10] we set $A=24.3$, and $B=0.7679$. The ground-state energy terms T, E_C, and E_{xc}, are calculated from the self-consistent set of eigenfunctions and energy eigenvalues according to the density-functional formalism.[15]

The second term in Eq. (1) represents the pressure correction due to the nonconstant potential between the MT spheres. It is the volume derivative of the energy E_{NMT} arising from the intersphere portion of the NMT crystal potential and electronic charge density. We approximate E_{NMT} following the method described by Danese and Connolly,[16] but for computational ease we neglect the contributions from the intrasphere NMT portion of the crystal potential and charge density. The actual intersphere charge density was approximated by a superposition of atomic charge densities produced in a Herman-Skillman[13] calculation using the $X\alpha$ exchange potential.[11] The value of α was chosen so that the amount of intersphere charge of this charge density equalled that of the self-consistent MT crystal charge density. Because of the close packing in CsI, P_{MT} is fairly small, amounting to approximately -0.2 GPa at low pressures, and -2.0 at 75 GPa. The magnitude of this pressure correction is not great enough to justify the additional computational effort required for a more rigorous treatment of the intersphere charge density and the inclusion of the smaller intrasphere pressure correction.

The final two contributions to Eq. (1), the zero-point pressure P_0 and the thermal pressure P_{th}, are computed using quasiharmonic lattice theory. Approximating the mean vibrational frequency of the crystal by the root-mean-squared frequency $\langle\omega^2\rangle^{1/2}$ one obtains[17]

$$P_0(v)=\gamma E_0(v)/v=3(\tfrac{3}{5})^{1/2}sk\gamma\Theta/2v \ . \tag{9}$$

$E_0(v)$ is the zero-point energy, s is the number of atoms per crystal basis, and k is Boltzmann's constant. The Debye temperature is given by[17]

$$\Theta(v)=\frac{h}{2\pi k}(5\langle\omega^2\rangle/3)^{1/2} \ , \tag{10}$$

where h is Planck's constant. The quasiharmonic Grüneisen parameter is[17]

$$\gamma(v)=-\frac{1}{3}\left|\frac{\partial\ln\Theta}{\partial\ln r}\right|_{r=r_{\text{equilibrium}}} \ , \tag{11}$$

where r is the interatomic separation. Since this $\gamma(v)$ is temperature independent, the lattice thermal pressure is given by

$$P_{\text{th}}(v,T)=\gamma E_{\text{th}}/v \ . \tag{12}$$

The Debye model is used to approximate the thermal energy, E_{th}. The theoretical room-temperature compression isotherm is shown in Fig. 1, with numerical values given in Table I.

B. Finite-strain effective pair potential

The mean-squared vibrational frequency used in Eqs. (10) and (11) is calculated from[18]

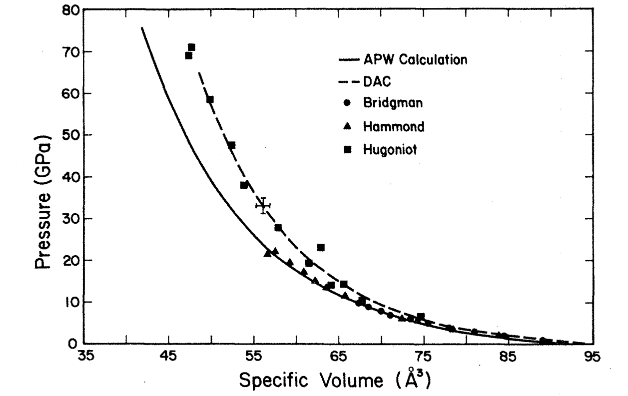

FIG. 1. Theoretical room-temperature isotherm of CsI (solid line) calculated from Eq. (1), compared with both static- and dynamic-compression data. The dashed line is Asaumi's (Ref. 29) fit to his DAC measurements. The representative error bar is adapted from the DAC measurements of Knittle and Jeanloz (Ref. 30), which are in excellent agreement with Asaumi's (Ref. 29) results. The static-compression measurements of Bridgman (Ref. 27) are given by the circles, and the DAC measurements of Hammond (Ref. 28) are given by the triangles. Note the close coincidence of the unreduced Hugoniot-curve data (squares) (Refs. 31—33) with the dashed line representing both Asaumi's (Ref. 29), and Knittle and Jeanloz's (Ref. 30) isotherm.

$$\langle\omega^2\rangle = \frac{1}{3s}\sum_{i,j}{}' \frac{1}{M_i}\nabla^2\phi_{ij}(r) \, . \tag{13}$$

M_i is the mass of the ith atom, and $\phi_{ij}(r)$ is the effective interatomic pair potential between the ith and jth atoms separated by the distance r. The summation is over all pair interactions involving each of the atoms in a particular unit cell, taken to be the "first" unit cell. For crystals with the NaCl or CsCl structure, in which the sublattices of each type of atom are equivalent, Eq. (13) reduces to

$$6\langle\omega^2\rangle/N = \frac{1}{M_1}\sum_{\text{atom 1}}{}' \nabla^2\phi_{1j}^{1-1} + \frac{1}{M_2}\sum_{\text{atom 2}}{}' \nabla^2\phi_{2k}^{2-2} + \left[\frac{1}{M_1}+\frac{1}{M_2}\right]\sum_{i\neq j}{}'\nabla^2\phi_{ij}^{1-2} \, . \tag{14}$$

The index j ranges over all atoms of type 1, except where the prime indicates that it is restricted from the first unit cell. The index k ranges similarly over all atoms of type 2. The superscripts on the pair potentials distinguish between the interactions of like and unlike atoms. If we assume $M_1 \approx M_2$, or that the effective potential field influencing each atom may be represented by an averaged field, then for these cubic crystals

$$\langle\omega^2\rangle = \frac{1}{6}\left[\frac{1}{M_1}+\frac{1}{M_2}\right]\nabla^2\Phi(r) \, , \tag{15}$$

TABLE I. Room-temperature (298 K) compression curve for CsI calculated from Eq. (1) using the corresponding theoretical values of $\langle\omega^2\rangle^{1/2}$, Θ, and γ calculated from Eqs. (21), (9), and (10), respectively. The static-lattice pressure is given by the first two terms in Eq. (1), $P_{\text{APW}}+P_{\text{MT}}$.

Volume (Å³)	$\langle\omega^2\rangle^{1/2}$ (10^{13} Hz)	Θ (K)	γ	Pressure Static (GPa)	Pressure $T=298$ K (GPa)
94.44	1.000	98.7	2.120	−0.75±0.1	−0.19±0.1
92.89[a]	1.036	102	2.034		0.0
89.96	1.122	111	1.939	0.0	
85.86	1.207	119	1.840	0.66±0.11	1.19±0.11
75.56	1.502	148	1.606	3.98±0.13	4.51±0.13
72.65	1.599	158	1.553	5.41±0.13	5.94±0.13
69.96	1.694	167	1.509	7.05±0.14	7.59±0.14
65.13	1.881	186	1.436	10.91±0.16	11.46±0.16
60.93	2.067	204	1.381	15.58±0.19	16.15±0.19
59.03	2.158	213	1.357	18.26±0.20	18.84±0.20
57.24	2.250	222	1.336	21.17±0.22	21.76±0.22
55.56	2.341	231	1.317	24.30±0.23	24.90±0.23
53.97	2.431	240	1.300	27.66±0.25	28.27±0.25
52.47	2.521	249	1.284	31.22±0.27	31.85±0.27
51.05	2.611	257	1.270	35.05±0.29	35.69±0.29
49.71	2.700	266	1.256	39.09±0.31	39.74±0.31
48.43	2.789	275	1.244	43.41±0.33	44.07±0.34
47.22	2.878	284	1.233	47.97±0.36	48.64±0.36
46.07	2.967	293	1.222	52.79±0.38	53.48±0.38
44.97	3.055	301	1.212	57.91±0.41	58.61±0.41
43.93	3.143	310	1.203	63.11±0.44	63.82±0.44
42.93	3.231	319	1.194	68.80±0.47	69.53±0.47
41.98	3.319	327	1.186	74.6 ±0.50	75.3 ±0.50

[a] Experimental zero-pressure volume = 95.32 Å³.

where Φ denotes the potential energy per unit cell. This mass weighting averaging of Eq. (13) renders Eq. (11) equivalent to the Vashchenko-Zubarev[19] formula for the Grüneisen parameter, as can be seen by comparison with Eq. (15) of Ref. 19. We have used Eq. (15) for our calculation rather than carry out the lattice sums in Eq. (13), since, for CsI, setting each of the atomic masses equal to their average is a good approximation. For alkali halides in general, where the largest contribution to the lattice sum of non-Coulomb interactions arises from the unlike atoms in the first shell of neighbors, one might expect only a small error would be introduced by the inexact treatment of like atom interactions when all interactions are assumed to be equivalent.

To produce a crystal potential to use in Eq. (15), we first obtain a third-order finite-strain fit to the static-lattice EOS $(P_{\mathrm{APW}}+P_{\mathrm{MT}})$ using a generalized definition of Birch's strain parameter[20,21] f,

$$f=\frac{2}{m}[(v_0/v)^{m/6}-1]\ . \tag{16}$$

v_0 is the $P=0$ volume. A particular measure of strain is determined by specifying the value of the parameter m. For example, for $m=4$, f is the Eulerian strain, and for $m=-4$, f is the Lagrangian strain. Making the usual assumption that the crystal potential energy can be written as a polynomial in strain, the finite-strain expression for the corresponding pressure is

$$P=3K_0f\left[\frac{mf}{2}+1\right]^{(m+6)/m}(1-2\xi f+4\zeta f^2+\cdots) \tag{17}$$

with

$$\xi=\tfrac{3}{8}(m+4-2K_0') \tag{18a}$$

and

$$\zeta=\tfrac{3}{8}[K_0K_0''+K_0'(K_0'-m-3)+3+2m+11m^2/36]\ . \tag{18b}$$

In Eqs. (18) K_0 is the $P=0$ value of the bulk modulus. K_0' and K_0'' are its first two pressure derivatives. Writing the crystal energy as a quartic in strain leads to the fourth-order finite-strain pressure equation, obtained from Eq. (17) by truncating the series after the term in f^2. The third-order finite-strain equation is obtained by truncating the series in (17) after the term in f. Defining F by analogy to Birch,[21] as

$$\begin{aligned}F&\equiv\frac{P}{3f[(mf/2)+1]^{(m+6)/m}}\\&=K_0(1-2\xi f+\zeta f^2+\cdots)\ ,\end{aligned} \tag{19}$$

the best least-squares values for v_0, K_0, K_0', and K_0'' can be easily determined from a polynomial fit to pressure-volume data. Following the procedure described by Bukowinski and Lees,[20] we choose m so that we obtain the fastest converging expansion for the crystal potential as a polynomial in strain. For this choice of m, the trend of the computed pressure values plotted as F vs f is indistinguishable from a straight line. We are thus able to use a third-order fit (F linear in f) that is as accurate as the fourth-order fit, and avoids the possible trade off between the order of a polynomial and the values of the coefficients.

For positive m the expansion of the crystal potential energy as a polynomial in f is equivalent to expressing the effective pair potential as a finite series in inverse powers of r. Rewriting Φ, given as a cubic in f, in terms of the specific volume, yields

$$\Phi(v)=3v_0\left[\frac{2A_1}{m}\left[\frac{v_0}{v}\right]^{m/6}+\frac{A_2}{m}\left[\frac{v_0}{v}\right]^{m/3}+\frac{2A_3}{3m}\left[\frac{v_0}{v}\right]^{m/2}\right]\ . \tag{20}$$

The coefficients A_l are given by

$$\begin{aligned}A_1&=-6K_0(1+4\xi/m)/m\ ,\\A_2&=6K_0(1+8\xi/m)/m\ ,\\A_3&=-24\xi K_0/m^2\ .\end{aligned} \tag{21}$$

Substituting Eq. (20) into Eq. (15) leads to the following expression for the mean-squared frequency:

$$\langle\omega^2\rangle=\frac{v_0}{2r^2}\left[\frac{1}{M_1}+\frac{1}{M_2}\right]\left[\frac{A_1(m-2)}{2}\left[\frac{v_0}{v}\right]^{m/6}+A_2(m-1)\left[\frac{v_0}{v}\right]^{m/3}+\frac{A_3(3m-2)}{2}\left[\frac{v_0}{v}\right]^{m/2}\right]\ . \tag{22}$$

In earlier work on NaCl,[22] where we have used both the crystal potential obtained from Eq. (20) and Born-Mayer-type[23] pair potentials, we have found that the values of γ and Θ calculated using Eq. (15) are sensitive to how well the potential model reproduces the compression curve, but not significantly sensitive to the mathematical form of the effective interatomic pair potential. Since we can routinely obtain very accurate fits to the theoretical compression points from the generalized finite-strain expression Eq. (19), we have used Eq. (22) in Eqs. (10) and (11) to generate Θ and γ. Values for $\langle\omega^2\rangle^{1/2}$, Θ, and γ are given in Table I.

III. RESULTS

A. Room-temperature compression curve

The calculated isotherm [Eq. (1)] is tabulated in Table I and shown in Fig. 1. Calculated room-temperature values of A_0, the equilibrium lattice constant, K_0, K_0', and K_0'', were determined from the same generalized finite-strain analysis applied to the static-lattice results earlier. Table II shows that the resulting parameter values agree well with the isothermal zero-pressure properties Barsch and Chang[24] determined from ultrasonic measurements. Uncertainties in our theoretical isotherm arise from the approximations inherent in the APW method, computational error, and our use of Debye theory and quasiharmonic lattice dynamics which neglect the temperature dependence of γ and provide a volume dependence that is untested by experiment. The theoretical zero-pressure values for Θ and γ (Table I) agree well with the experimentally determined values 101 K and 2.0±0.30, respectively,[25,26] but the observed anharmonic effects at temperatures greater than 225 K suggest the need for accounting for the explicit dependence on temperature.[25] We have no means of estimating the uncertainty arising from the approximations inherent in the APW method.

In addition to the theoretical isotherm, Fig. 1 includes static-compression measurements of Bridgman,[27] DAC measurements of Hammond,[28] and Asaumi's[29] fit of the third-order Birch-Murnaghan finite-strain equation [Eq. (16) with $m=4$, truncated after the term in f] to his recent DAC measurements. The representative error bar shown on this fit is adapted from a second set of recent DAC measurements of Knittle and Jeanloz,[30] which are in excellent agreement with Asaumi's[29] results. Shown for comparison is the Hugoniot curve (the unreduced shock compression data) for CsI.[31–33] At low pressures our isotherm is in good agreement with all of the static-compression measurements. At higher pressures the theoretical isotherm continues to agree with the experimental data of Bridgman[27] and Hammond,[28] but it is significantly softer than the DAC measurements of Asaumi,[29] and Knittle and Jeanloz.[30]

The isotherms measured by Asaumi,[29] and Knittle and Jeanloz[30] closely coincide with the Hugoniot curve of CsI, which comprises four independent sets of measurements.[31–33] This agreement between the isotherm and the Hugoniot curve implies that γ is effectively zero along the Hugoniot curve. Such a condition could arise from thermal excitation of electrons, but from our calculations of the Hugoniot curve, given below, we find it difficult to reconcile the coincidence of these isotherms and the Hugoniot curve.

B. Energy band-gap volume dependence

Herzfeld's theory of metallization predicts that CsI should become metallic at a specific volume of 24.3 cm^3/mole (40.3 Å^3/cell).[4] Using our theoretical isotherm the predicted metallization pressure is 87 GPa. A precise estimate of the metallization pressure is difficult to obtain from Asaumi and Kondo's[8] optical-absorption measurements. A suitable procedure for identifing the energy at which absorption sets in is not readily apparent. Asaumi *et al.*[34] have chosen this threshold energy E_t as the energy at which the optical density equals 0.10. Syassen's[5] procedure of fitting experimental results to the relation between absorption and band gap for transitions between parabolic bands may provide more meaningful values for E_t. In alkali halides the optical-absorption edge is marked by a series of excitonic peaks in the absorption spectrum.[35] Thus the uncertainty in identifying the E_t is augmented by the uncertainty in the relation of E_g to E_t. In the case of a direct band gap, Asaumi and Kondo[8] originally assumed $E_g = E_t + 0.6$ eV, but have revised[29] this relation to the proportionality $E_g = 1.26E_t$. The proportionality constant is the ratio of the $P=0$ band gap, determined independently, to the zero-pressure value of E_t. Owing to these ambiguities in the interpretation, we believe their data probably does not constrain the band gap to better than ±0.5 eV.

Using the computed equation of state to plot Asaumi and Kondo's threshold energies as a function of volume rather than pressure facilitates graphic extrapolation of E_g to band-gap closure, as shown in Fig. 2. The two ex-

TABLE II. The zero-pressure properties of the theoretical room-temperature (298 K) isotherm compared with the isothermal values determined from acoustic measurements at pressures up to 1 GPa (Ref. 4) A_0 is the equilibrium lattice constant, K_0 is the zero-pressure bulk modulus, and K_0' and K_0'' are its first- and second-pressure derivatives, respectively.

	APW calculation	Barsch and Chang[a]
Density (g/cm^3)	4.645±0.030	4.525±0.014
A_0 (Å)	4.529±0.010	4.568±0.014[b]
K_0 (GPa)	11.95±0.44	11.89±0.05
K_0'	6.14±0.22	5.93±0.08
K_0'' (GPa^{-1})	−1.29±0.19	−0.73±0.08

[a] Reference 4.

[b] Reference 24.

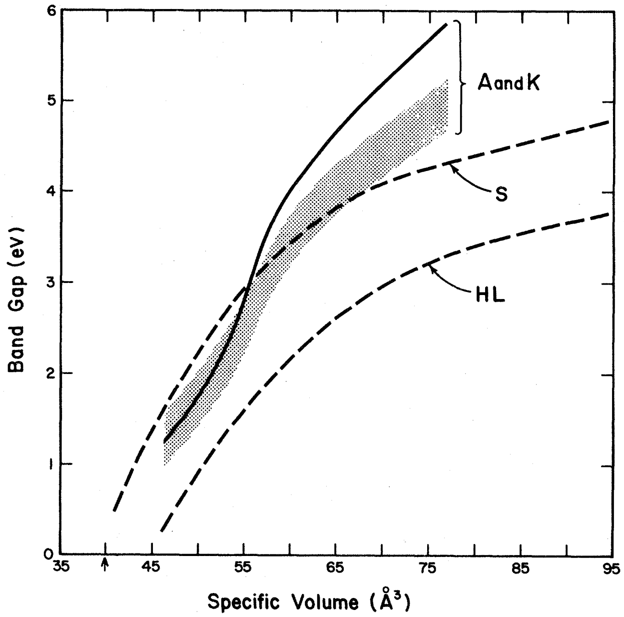

FIG. 2. Volume dependence of the energy band gap in CsI. The extremes of the shaded region correspond to Asaumi and Kondo's[8] (A and K) estimate of the magnitude of a direct gap (upper edge) and an indirect gap (lower edge). The solid line is their revised (Ref. 34) estimate of the band gap. The upper dashed line (S) is produced from the APW calculation using the Slater exchange potential, and the lower dashed line (HL) is produced using the HL potential. The theoretical isotherm from Fig. 1 was used to convert the observed pressure values into volumes. The arrow at 40 Å^3 marks the volume of metallization predicted by Herzfeld's theory (Ref. 3).

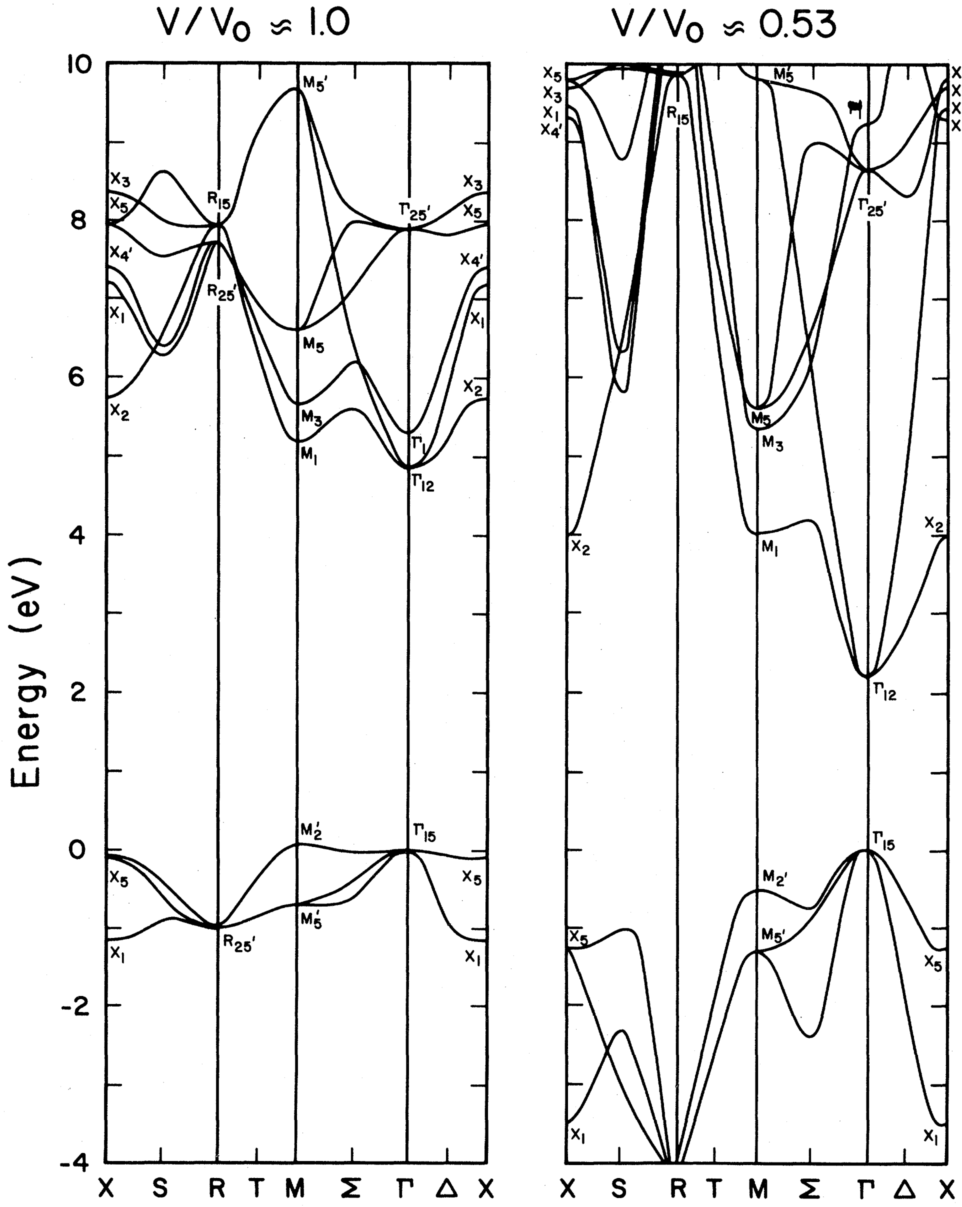

FIG. 3. Electronic band structure of CsI in the (110) and (100) directions, and on the Brillouin-zone boundary along the face diagonal and edge. The band structure is shown at two compressions: near zero pressure ($v/v_0 \approx 1.0$) and near 40 GPa ($v/v_0 \approx 0.53$). The energies are relative to the valence Γ_{15} state at 0 eV. Note the reordering and marked broadening of the bands, and the accompanying reduction in the band gap at Γ.

tremes of the shaded region correspond to Asaumi and Kondo's[8] two estimates for E_g. The upper edge assumes a direct gap, and the lower an indirect gap. The solid line is their revised[29] estimate of E_g. Also included in this figure are the two theoretical estimates of E_g at 0 K produced by the HL and Slater APW calculations. These are shown by the dashed lines. The detailed band structure at two compressions in Fig. 3 illustrates the reordering of the bands as well as the reduction of the band gap. Although density-functional eigenvalues do not represent actual excitation energies, it might be expected that as the gap gets smaller, and as the electronic density increases, the error due to the one-body approximation diminishes. This is corroborated by our results: At zero pressure both exchange-correlation models significantly underestimate the band gap, while at high pressure they bracket the experimental values. Thus even allowing for experimental uncertainties there is considerable consistency between experiment and theory at high pressures.

Allowing an uncertainty of ±0.5 eV in Asaumi and Kondo's absorption edge bounds, graphical extrapolation to zero gap yields a metallization volume in the range 38—46 Å^3 and a corresponding pressure range of 53—116 GPa. The APW calculations would predict the metallization of CsI to occur at a volume of 45.5 Å^3 and 55 GPa using the HL potential, and 38.5 Å^3 and 100 GPa using the Slater potential. The relationship between the calculated and experimental band gaps for CsI is very similar to that observed in Xe.[2,5] The theoretical band gap at high pressure is direct between the p-like iodine Γ_{15} state and the d-like cesium Γ_{12} state (Fig. 3) suggesting that the APW values should be compared with the upper limit of the measured threshold energies. We conclude that the metallization pressure is likely to fall in the range (100 ± 10) GPa, assuming the suspected structural phase transitions[29,30] have negligible effect on the band gap. This result is somewhat higher than Asaumi and Kondo's estimate,[8,29] but corresponds well to the specific volume of metallization predicted by Herzfeld's theory.[3]

C. Shock-compression curve

The high temperatures generated by shock waves make it necessary to account for the energy of the shock that is partitioned among the thermally excited electrons in the conduction band.[32,36] Accordingly, we have calculated shock-compression curves for CsI following the method used by Ross and co-workers[5,37] for Xe. Previous calculations for CsI used a volume-independent band gap[33] and a predetermined pair-interaction potential with parameters fitted to the Hugoniot curve. Our calculations use the results of the APW calculations for the potential and the volume-dependent band gap.

Following Ross and McMahan[2] we seek the locus of points satisfying the Hugoniot-curve equation:

$$E_H(v,T)-E(v_0,298\text{ K}) = \tfrac{1}{2}[P_H(v,T)+P(v_0,298\text{ K})](v_0-v)\ . \tag{23}$$

Five contributions to the unit-cell energy are considered,

$$E_H(v,T)=\Phi(v)+E_0(v)+E_{\text{th}}(v,\Theta) +N_e(v,T)[E_g(v)+3kT]\ . \tag{24}$$

Onto the static-lattice energy Φ we add the zero-point energy E_0 and the thermal energy E_{th} calculated as in Eq. (8) and Eq. (11), respectively. The final two terms in Eq. (23) are the energy absorbed per excited electron, taken to be equal to the energy-band gap E_g, plus the kinetic energy of the essentially free electrons and holes occupying the conduction and valence bands, respectively. The number of excited electrons per unit cell N_e is expected to be substantial under shock conditions. Therefore, the law of mass action for semiconductors[38] does not provide a rigorous estimate of N_e. We make the following simple estimate of the effect of electron excitations for the purpose of illustration.

We begin by extending the usual result for the law of mass action[38] to obtain a better estimate of N_e and $E_g/2kT \lesssim 1$. As in the standard development, we treat the energy bands as being parabolic in the vicinity of the band edges. Expanding the Fermi distribution function in powers of $\exp[-(E-\mu)/kT]$, where E is the energy and μ the chemical potential, the integration of the density of states weighted by the Fermi distribution can be carried out explicitly. We approximate μ by the Fermi energy E_F which is its zero-temperature value. For an intrinsic semiconductor the concentration of conduction electrons per unit cell is given by

$$N_e(v,T)=2v(g_v g_c)^{1/2}\left[\frac{2\pi kT(m_v m_c)^{1/2}}{h^2}\right]^{3/2} \times \sum_{x=1}^{\infty}(-1)^{x+1}x^{-3/2}\exp(-xE_g/2kT)\ . \tag{25}$$

$g_{V,C}$ is the degeneracy of the edge of the valence or conduction bands, respectively, and similarly $m_{V,C}$ is the effective mass of these bands. In our calculations of shock-compression curves for CsI we take the energy-band gap to be direct (Γ_{12}-Γ_{15}), as suggested by the APW calculations, and set $g_c=2$ and $g_v=3$. Both effective masses are set equal to the free-electron rest mass, and we retain all terms in the summation in Eq. (25) that contribute at least 1% of its total value. In the limit $E_g/2kT \gg 1$, keeping only the first term in the summation in Eq. (25) leads to the standard expression.[2] This "one-term" approximation does not rely on the assumption $\mu=E_F$, but is systematically produces larger values for the concentration of conduction electrons than does Eq. (25).

In Eq. (23), we considered the contributions to the internal pressure arising from the energy terms in Eq. (24):

$$P_H(v,T)=P(v,T)+N_e(v,T)\left[\frac{2kT}{v}-\frac{\partial E_g}{\partial v}\right]\ . \tag{26}$$

The first term contains the static-lattice, zero-point, and lattice-thermal contributions to the pressure at the Hugoniot state, and is calculated as in Eq. (1). The contribution to the internal pressure from the gas of conduction electrons and valence holes is given by the first term in large parentheses. The last term in Eq. (26) corresponds to the change of pressure caused by the excitation of electrons from the valence band to the conduction band. For CsI the band gap is decreasing with volume ($\partial E_g/\partial v>0$) making this last term a negative contribution and leading to a softening of the Hugoniot curve.

In Fig. 4(a) the shock data for CsI (Ref. 31–33) are compared with the theoretical Hugoniot curves calculated from Eq. (23) using a variety of hypothetical volume dependencies for E_g. The Hugoniot curve labeled INS was calculated without including electronic excitations (the pure insulator case). Curves S and HL were computed using the band gaps from the Slater and HL calculations, respectively, both of which are shown in Fig. 2. For comparison, curve C results from using a constant band gap of 6.4 eV, which is it's $P=0$ value,[12] and curve L is calculated using a band gap starting at 6.4 eV and decreasing linearly to 0 eV at 40 Å^3. These latter results are in reasonably good agreement with experiment. Given the physical conditions and complexity of the problem, these band gaps should be regarded as effective. A more complete theory would treat the system as a dense plasma with the energy levels, electron occupation numbers, chemical potential, and atomic correlations being calculated self-consistently. Such a calculation is not warranted given the uncertainties in the experimental data. Figure 5 contains some of the calculated values of T and N_e along the Hugoniot curve. At pressures near 100 GPa, $E_g/2kT\approx 1$, the present model [Eq. (25)] is only very approximate.

An error of 2% in volume[37] has been assigned to the

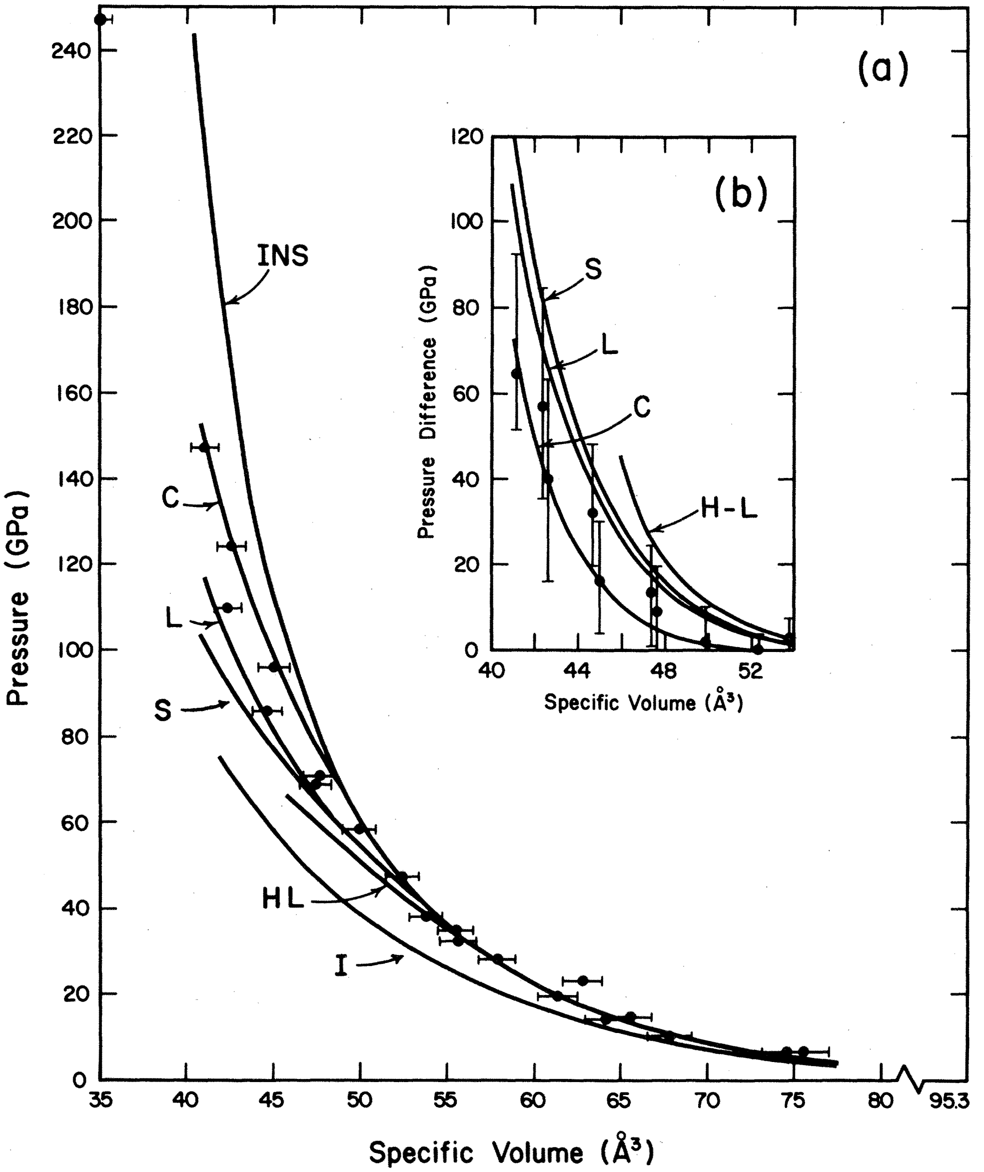

FIG. 4. (a) Comparison of theoretical Hugoniot curves calculated from Eq. (22) with experimental-shock data (Refs. 31–33). An uncertainty in volume of 2% (Ref. 37) has been added to the experimental values. Curve INS is for the pure insulator. The calculations for semiconducting CsI used a constant band gap of 6.4 eV (curve *C*); a linearly varying band gap starting at 6.4 eV at v_0 and decreasing to 0 eV at 40 Å^3 (curve *L*); the band gap from the Slater calculation (curve *S*); and the band gap from the HL calculation (curve HL). Curve *I* is the theoretical isotherm from Fig. 1. (b) (Inset) The shock-compression data and Hugoniot curves for semiconducting CsI from (a) replotted relative to the curve calculated for the pure insulator. The uncertainty in volume assigned in (a) has been propagated into this figure as an uncertainty in pressure.

shock data to provide a qualitative illustration of the uncertainty of these measurements. To amplify the effect of excitations on the Hugoniot curve, these data and the Hugoniot curves for semiconducting CsI have been replotted in Fig. 4(b) relative to the pressure calculated for a pure insulator. The 2% uncertainty assigned to the shock data in Fig. 4(a) has been propagated into Fig. 4(b) as an uncertainty in the pressure difference. Even with the estimated uncertainty the experimental Hugoniot-curve data are significantly reduced from the pure-insulator calculation. Within the accuracy of our simple model, the trend of this offset can be adequately explained in terms of excitations of electrons across a constant band gap or a band gap that decreases linearly with volume. Neither the data nor the theory are sufficiently precise to distinguish between the theoretical models.

Also plotted in Fig. 4(a) is the theoretical APW isotherm from Fig. 1, labeled *I*. The additional thermal pressure in the shocked state gives rise to the difference between the Hugoniot curve and this isotherm. This thermal pressure would be present whether we used the APW or an experimental isotherm as our "cold curve." The substantial amount of thermal pressure at all densities makes it difficult to understand why the recent DAC measurements[29,30] are coincident with the Hugoniot curve. As we have noted, this coincidence requires that the effective

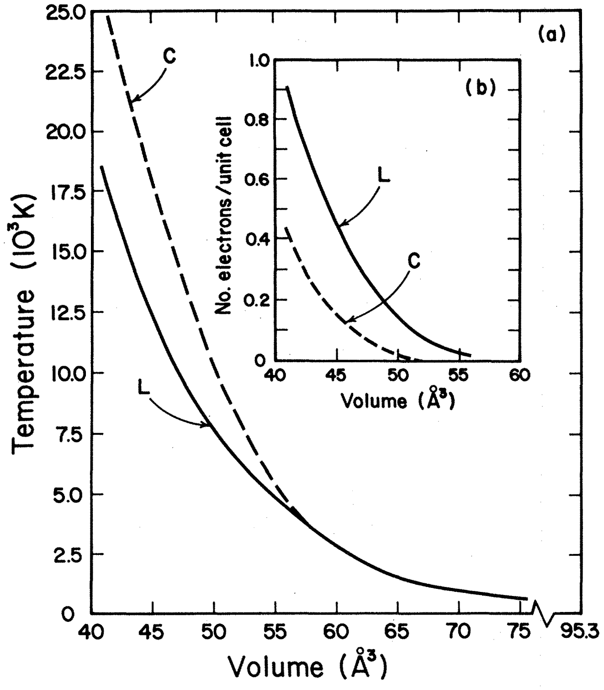

FIG. 5. Values of T and N_e (inset) along the Hugoniot curve calculated from Eqs. (22)–(25) using two effective band gaps. The solid lines (L) result from using a band gap varying linearly from 6.4 eV at v_0 and decreasing to 0 eV at 40 Å^3. The dashed lines (C) result from using a constant band gap of 6.4 eV.

γ (electronic plus lattice) must be zero. This could possibly occur when there is a substantial amount of electronic excitations. However, the results in Fig. 5 show that at 55 Å^3, for example, the amount of electronic excitations is small and the temperature is about 5000 K, which leads to a thermal pressure of about 10 GPa. At this volume, then, the isotherm and Hugoniot curve should be offset by this amount.

IV. DISCUSSION

The similarity of the electronic configuration in Xe, CsI, and BaTe suggests that their band structures and properties may demonstrate systematic behavior. Figure 6 shows some of the measured optical gaps for those compounds[5,6,8,39] plotted versus the natural logarithm of the reduced volume (v/v_H). Here v is the actual volume and v_H is the gap closure volume predicted by the Herzfeld model. The data follow a systematic trend which reflects the similarity of their electronic structure. Note that the band gaps at $P=0$ fall virtually on the same curve as those of the compressed materials. At ambient conditions each are at different stages along the IMT transition and the application of pressure effectively transforms one into another. Although the closing gap is direct in CsI and indirect in Xe, in both cases the empty band is d like and the metallization in both may be characterized as a p-d transition.

The isoelectronic structure of Xe and CsI is also reflected in their computed EOS. We expect the additional Coulomb interaction in CsI to shorten the nearest-

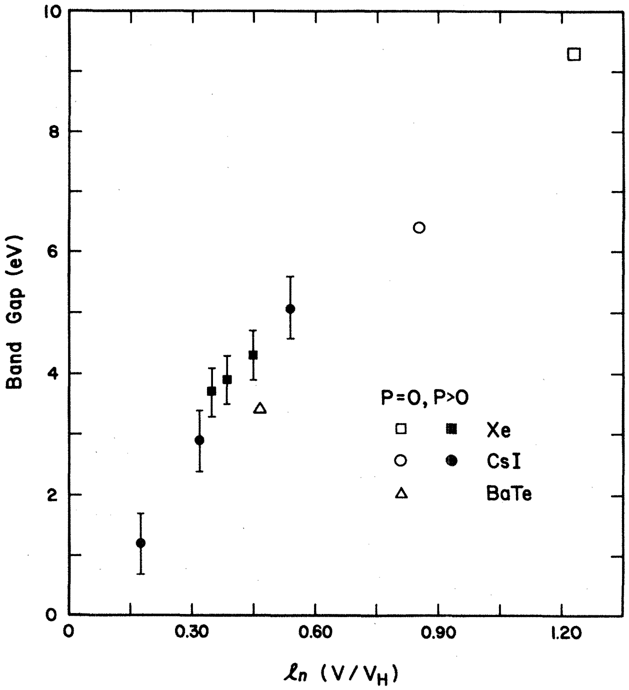

FIG. 6. The systematic variation of the band gap in the isoelectronic series Xe, CsI, and BaTe plotted against the natural logarithm of the specific volume normalized by the metallization volume predicted by Herzfeld's theory (Ref. 3) v_H. The $P=0$ values are denoted by the open symbols. The value for BaTe was estimated from the optical measurements of Zollweg (Ref. 39). The zero-pressure band gap in CsI is taken from Ref. 12. The other CsI data is from the revised analysis (Ref. 34) of optical measurements (Ref. 8), and the Xe data is from Refs. 5 and 6.

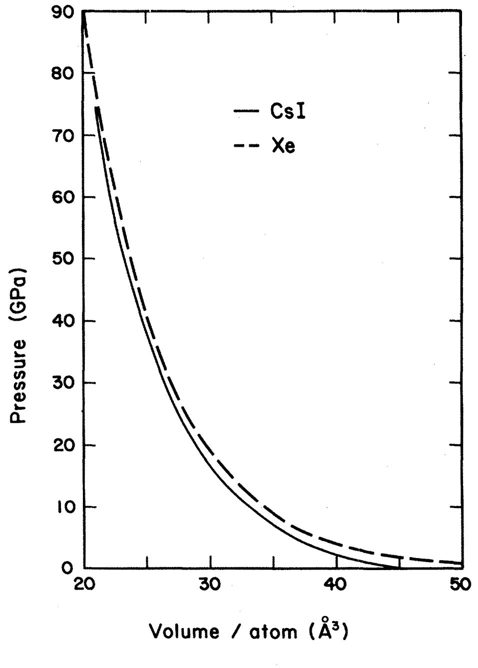

FIG. 7. Static-lattice EOS of CsI (solid line) and Xe (dashed line) as calculated by the APW method (this work and Ref. 5), and plotted on a per-atom basis.

neighbor distance. Hence in the solid, we expect CsI to be denser than Xe at a given pressure. This difference should become proportionately smaller at high pressure, where repulsive interactions dominate. As is shown in Fig. 7, the calculated EOS's are related in the expected way. Since the Xe EOS agrees closely with recent DAC measurements,[40] this increases our confidence that the CsI EOS remains accurate at high pressure. Although the calculations for Xe were made for a fcc lattice, while in the CsI structure the atoms are in bcc packing, the p-v curves for these two close-packed structures are known to differ only slightly.

If BaTe follows the same pattern, then the Herzfeld model predicts that it will become metallic at approximately 30 GPa (corresponding to $v_H = 32.2$ cm^3/mole or 26.7 Å^3/atom). We have made some preliminary calculations of the band structure of BaTe in the *B*1 (NaCl) phase. The predicted metallization volumes according to the Slater and HL exchange-correlation potentials bracket the Herzfeld volume v_H. However, recent high-pressure x-ray and optical studies of BaTe indicate that it transforms to the *B*2 (CsCl) structure at approximately 4.8 GPa.[41] Previous calculations of pressure effects on the band structure of CaO predict that the *B*2 phase should become metallic at a somewhat smaller specific volume than the *B*1 phase.[42] The metallization volume for the latter also agreed with the actual Herzfeld volume v_H. Hence we conclude that the actual metallization pressure of BaTe may be somewhat higher than 30 GPa. On reviewing the present work on CsI we conclude that a major barrier to a quantitative understanding of the EOS is the apparent discrepancy between the several sets of isothermal measurements.

Note added in proof. Huang and Ruoff[43] have just published a new experimental equation of state for CsI. They report that CsI transforms to a new crystallographic structure at 40 GPa. Below 40 GPa, their compressibility curve for CsI (*B*2) is consistent with our computed curve.

ACKNOWLEDGMENTS

One of us (J.A.) benefited greatly from discussions with George H. Wolf. We thank Dr. K. Asaumi and E. Knittle for providing us their optical and compression data in advance of publication. This work was supported by National Science Foundation Grant No. EAR-82-12392.

---

*Present address: SRI International, Menlo Park, CA 94025.

[1] M. Ross and A. K. McMahan, Phys. Rev. B 26, 4088 (1982).

[2] M. Ross and A. K. McMahan, Phys. Rev. B 21, 1658 (1980); W. J. Nellis, M. van Thiel, and A. C. Mitchell, Phys. Rev. Lett. 48, 816 (1982).

[3] K. F. Herzfeld, Phys. Rev. 29, 701 (1927).

[4] M. Ross, J. Chem. Phys. 56, 4561 (1972); M. Ross and A. K. McMahan, in *Physics of Solids Under High Pressure,* edited by J. S. Schilling and R. N. Shelton (North-Holland, Amsterdam, 1981), p. 161.

[5] K. Syassen, Phys. Rev. B 25, 6548 (1982).

[6] K. Asaumi, T. Mori and Y. Kondo, Phys. Rev. Lett. 49, 837 (1982).

[7] J. Aidun and M. S. T. Bukowinski, Solid State Commun. 47, 855 (1983).

[8] K. Asaumi and Y. Kondo, Solid State Commun. 40, 715 (1980).

[9] T. L. Loucks, *Augmented Plane Wave Method* (Benjamin, New York, 1967); L. F. Mattheiss, J. H. Wood, and A. C. Switendick, in *Methods in Computational Physics,* edited by B. Alder, S. Fernback, and M. Rotenberg (Academic, New York, 1968), Vol. 8, p. 63.

[10] L. Hedin and B. I. Lundqvist, J. Phys. C 4, 2064 (1971); B. I. Lundqvist and S. Lundqvist, in *Computational Solid State Physics,* edited by F. Herman, N. W. Dalton, and T. R. Koehler (Plenum, New York, 1972), p. 219.

[11] J. C. Slater, *Quantum Theory of Molecules and Solids* (McGraw-Hill, New York, 1974), Vol. 4.

[12] Y. Onodera, J. Phys. Soc. Jpn. 25, 469 (1968).

[13] F. Herman and S. Skillman, *Atomic Structure Calculations* (Prentice-Hall, Englewood Cliffs, 1963).

[14] See, for example J. C. Slater, J. Chem. Phys. 61, 3063 (1974).

[15] P. Hohenberg and W. Kohn, Phys. Rev. 136, 864 (1964); W. Kohn and L. J. Sham, *ibid.* 140, 1133 (1965).

[16] J. B. Danese and J. W. D. Connolly, J. Chem. Phys. 61, 3063 (1974).

[17] D. C. Wallace, *Thermodynamics of Crystals* (Wiley, New York, 1972).

[18] A. A. Maradudin, E. W. Montroll, and C. H. Weiss, *Theory of Lattice Dynamics in the Harmonic Approximation* (Academic, New York, 1963).

[19] V. Ya. Vashchenko and V. N. Zubarev, Fiz. Tverd. Tela (Leningrad) 5, 886 (1963) [Sov. Phys.—Solid State 5, 653 (1963)].

[20] M. S. T. Bukowinski and A. C. Lees (unpublished).

[21] F. Birch, J. Geophys. Res. 83, 1257 (1978).

[22] J. Aidun (unpublished).

[23] M. P. Tosi and F. G. Fumi, J. Phys. Chem. Solids 25, 45 (1964); F. T. Smith, Phys. Rev. A 5, 1708 (1972); Y. Ida, Phys. Earth Planet. Inter. 13, 97 (1976); R. Narayan and S. Ramaseshan, Pramana 13, 581 (1979).

[24] G. R. Barsch and Z. P. Chang, in *Accurate Characterization of the High Pressure Environment,* edited by Edward C. Lloyd National Bureau of Standards Publication No. 326 (U.S. GPO, Washington, D.C., 1971), p. 173.

[25] A. D. Redmond and B. Yates, J. Phys. C 5, 1589 (1972).

[26] A. C. Bailey and B. Yates, Philos. Mag. 16, 1241 (1967).

[27] P. W. Bridgman, Proc. Am. Acad. Arts Sci. 76, 1 (1945).

[28] D. E. Hammond, M.S. thesis, University of Rochester, Rochester, New York, 1969.

[29] K. Asaumi, Institute of Solid State Physics (University of Tokyo) Technical Report Ser. A., No. 1336, 1983 (unpublished).

[30] E. Knittle, and R. Jeanloz, Science 223, 53 (1984).

[31] S. P. Marsh, LASL Shock Hugoniot Data, Los Alamos Scientific Laboratory, University of California, 1980 (unpublished); R. H. Christian, Ph.D. thesis, University of California, Lawrence Livermore National Laboratory, Livermore, California, 1957 (unpublished).

[32] V. L. Al'tshuler, M. N. Pavlovskii, I. V. Kuleshova, and G. V. Simakov, Fiz. Tverd. Tela (Leningrad) 5, 279 (1963) [Sov. Phys.—Solid State 5, 203 (1963)].

[33] M. N. Pavlovskii, V. Ya. Veshchenko and G. V. Simakov, Fiz. Tverd. Tela (Leningrad) 7, 1212 (1965) [Sov. Phys.—Solid

State 7, 972 (1965)].

[34] K. Asaumi (private communication); K. Asaumi, T. Suzuki and T. Mori, Institute of Solid State Physics (University of Tokyo) Technical Report Ser. A, No. 1301, 1983 (unpublished).

[35] K. Teegarden and G. Baldini, Phys. Rev. 155, 896 (1967).

[36] M. Ross, Phys. Rev. 171, 777 (1968).

[37] M. Ross, W. Nellis, and A. Mitchell, Chem. Phys. Lett. 68, 532 (1979).

[38] See, for example, N. W. Ashcroft and N. D. Mermin, *Solid State Physics* (Holt, Rinehart and Winston, New York, 1976).

[39] R. J. Zollweg, Phys. Rev. 111, 113 (1958).

[40] D. Schifferl, R. L. Mills, and L. E. Trimmer (unpublished).

[41] T. A. Grzybowski and A. L. Ruoff, in Proceedings of the 1983 AIRAPT (Association International for Research and Advancement of High Pressure Science and Technology) meeting, Albany, New York (1983) (unpublished).

[42] M. S. T. Bukowinski, J. Geophys. Res. 87, 303 (1982).

[43] T.-L. Huang and A. L. Ruoff, Phys. Rev. B 29, 1112 (1984).